Stanford Exploration Project, Report 115, May 22, 2004, pages 233–248

Velocity uncertainty in tomography

Robert G. Clapp[1]

ABSTRACT

The conventional method for migration velocity analysis scans over one (or possibly multiple) move-out parameter(s) ang the offset or angle axis. The appropriate move-out parameter is then selected based on what produces the best coherence. The coherence as a function of the scanning parameter provides important information on how confident we are of our given move-out measure. In this paper, the move-out parameter selection is set up as an inverse problem and multiple, equi-probable move-out fields are generated. These various realization of move-out are then used to update the velocity model and migrated image. Early results are promising.

INTRODUCTION

Risk assessment is a key component to any business decision. Geostatistics has recognized this need and has introduced methods such as simulation to attempt to assess uncertainty in their estimates of earth properties (Isaaks and Srivastava, 1989). The problem is that the geostatistical methods are generally concerned with local, rather than global, solutions to problems and therefore can not be easily applied to the global inversion problems that are common in geophysics.

In previous works (Clapp, 2000, 2001b,c), I showed how we can modify standard geophysical inverse techniques by adding random noise into the model styling goal to obtain multiple realizations. In Clapp (2002a) and Chen and Clapp (2002), these multiple realizations were used to produce a series of equi-probable velocity models. The velocity models were used in a series of migrations, and the effect on Amplitude vs. Angle (AVA) was analyzed. In Clapp (2003a), I showed how the data fitting goal can be modified to account for data uncertainty. I demonstrated its applicability to a simple Super Dix (Clapp et al., 1998) problem.

In this paper I extend the data uncertainty concept to a ray based tomography problem (Stork and Clayton, 1991; Clapp, 2001b). I show how we can produce multiple, realistic velocity models. On a complex synthetic I produce a range of equi-probable velocity models, for migration to produce kinetically different images.

[1]**email:** bob@sep.stanford.edu

MULTIPLE REALIZATIONS REVIEW

Inverse problems obtain an estimate of a model $\mathbf{m}$, given some data $\mathbf{d}$ and an operator $\mathbf{L}$ relating the two. We can write our estimate of the model as minimizing the objective function in a least-squares sense,

$$f(\mathbf{m}) = \|\mathbf{d} - \mathbf{L}\mathbf{m}\|^2. \tag{1}$$

We can think of this same minimization in terms of fitting goals as

$$\mathbf{0} \approx \mathbf{r} = \mathbf{d} - \mathbf{L}\mathbf{m}, \tag{2}$$

where $\mathbf{r}$ is a residual vector.

Bayesian theory tells us (Tarantola, 1987) that convergence rate and the final quality of the model is improved the closer $\mathbf{r}$ is to being Independent Identically Distributed (IID). If we include the inverse noise covariance $\mathbf{N}$ in our inversion our data residual becomes IID,

$$\mathbf{0} \approx \mathbf{r} = \mathbf{N}(\mathbf{d} - \mathbf{L}\mathbf{m}). \tag{3}$$

A regularized inversion problem can be thought of as a more complicated version of (3) with an expanded data vector and an additional covariance operator,

$$\begin{aligned} \mathbf{0} &\approx \mathbf{r_d} = \mathbf{N_{noise}}(\mathbf{d} - \mathbf{L}\mathbf{m}) \\ \mathbf{0} &\approx \mathbf{r_m} = \epsilon \mathbf{N_{model}}(\mathbf{0} - \mathbf{I}\mathbf{m}). \end{aligned} \tag{4}$$

In this new formulation, the first expression is the "data fitting goal" and the second is the "model styling goal", $\mathbf{r_d}$ is the residual from the data fitting goal, $\mathbf{r_m}$ is the residual from the model styling goal, $\mathbf{N_{noise}}$ is the inverse noise covariance, $\mathbf{N_{model}}$ is the inverse model covariance, $\mathbf{I}$ is the identity matrix, and ϵ is a scalar that balances the fitting goals against each other. Normally we think of $\mathbf{N}_{\text{model}}$ as the regularization operator $\mathbf{A}$. Simple linear algebra leads to a more standard set of fitting goals:

$$\begin{aligned} \mathbf{0} &\approx \mathbf{r_d} = \mathbf{N}_{\text{noise}}(\mathbf{d} - \mathbf{L}\mathbf{m}) \\ \mathbf{0} &\approx \mathbf{r_m} = \epsilon \mathbf{A}\mathbf{m}. \end{aligned} \tag{5}$$

A problem with this approach is that we never know the true inverse noise or model covariance and therefore are only capable of applying approximate forms of these matrices.

One way to approximate $\mathbf{N}_{\text{noise}}$ is to think of it as a chain of two operators (Clapp, 2003a). One operator will describe the two-point covariance of the matrix $\mathbf{N_{n,c}}$ and one operator that describes the variance $\mathbf{N_{n,v}}$. We have a number of options in designing $\mathbf{N_{n,c}}$. We can use a Laplacian or some type of symmetric operator, a stationary Prediction Error Filter (Claerbout, 1999), a steering filter (Clapp, 2001b), or a non-stationary PEF (NSPEF) (Crawley, 2000). What we use is based on our *a priori* knowledge of our noise. The variance component $\mathbf{N_{n,v}}$ can be thought of simply in terms on how reliable we consider a given component of our data.

A simple example of this is the Super Dix (Clapp and Biondi, 1999) problem where $\mathbf{N_{n,v}}$ is constructed from stack power.

Another problem with fitting goals (5) is that we produce a single answer, with no information on the variability of different components in the model space. Our single answer is the minimum energy solution. In (Clapp, 2001b) I showed how, for the interpolation problem, we can produce a range of equi-probable solutions by replacing $\mathbf{r_m}$ with a random noise vector $\mathbf{n}$. The resulting models all had a more realistic texture than the minimum energy solution because the regularization operator did not fully describe the inverse model covariance.

In (Clapp, 2003a) I showed, how by replacing $\mathbf{r_d}$ with a random noise vector, we could produce a range of equi-probably interval velocity estimates for the Super Dix problem. The Super Dix example was a 1-D problem. The $\mathbf{N_{n,c}}$ was a derivative operator. The $\mathbf{N_{n,v}}$ operator was constructed based on the semblance scan. The variance was based on how quickly the semblance fell off from the peak value used to construct the data. The resulting models provided a fuller description of the potential interval velocity models but the 1-D nature of the problem limited its usefulness. A more interesting implementation of the methodology is the migration velocity analysis problem.

TOMOGRAPHY REVIEW

Tomography for migration velocity analysis is a non-linear problem that we linearize around an initial slowness model. In this discussion, I will be talking about the specific case of ray based tomography but most of the discussion is valid for other tomographic operators. We can linearize the problem around an initial slowness model and obtain a linear relation $\mathbf{T}$ between the change in travel times $\Delta\mathbf{t}$ and change in slowness $\Delta\mathbf{s}$:

$$\Delta\mathbf{t} \approx \mathbf{T}\Delta\mathbf{s}. \tag{6}$$

Certain components of the velocity model are better determined than others. As a result we need to either choose an intelligent model parameterization (Cox et al., 2003) or regularize the model. I prefer the regularizing approach so that I can easily incorporate *a priori* information. I impose a regularization operator that tends to smooth the velocity according to reflector dip (Clapp, 2001b). My resulting fitting goals then become

$$\begin{aligned} \Delta\mathbf{t} &\approx \mathbf{T}\Delta\mathbf{s} \\ \mathbf{0} &\approx \mathbf{A}(\mathbf{s_0}+\Delta\mathbf{s}). \end{aligned} \tag{7}$$

where $\mathbf{A}$ is a steering filter. In this paper I will do downward continuation based migration (Stoffa et al., 1990; Ristow and Ruhl, 1994) and then constructing angle gathers (Prucha et al., 1999; Sava and Fomel, 2000). Biondi and Symes (2003) and Biondi and Tisserant (2004) showed that the travel time error is related to the reflector dip α, local slowness $\mathbf{s_0}$, depth z_0, and the velocity model scaled by γ through

$$\Delta\mathbf{t}_{\text{RMO}} = \frac{1-\rho}{\cos\alpha}\frac{\sin^2\gamma}{\left(\cos^2\alpha-\sin^2\gamma\right)}s_0 z_0. \tag{8}$$

One of the best ways to scan over γ is by doing Stolt Residual Migration (SRM) (Sava, 1999b,a). In Clapp (2002b) I showed how we can obtain better ray-based tomography results by doing SRM scanning versus simple vertical move-out analysis.

THEORY

My goal in this paper is to produce multiple, equi-probable velocity models. A straight forward implementation of the approach described above, just accounting for data uncertainty, would lead to the fitting goals,

$$\begin{aligned} \mathbf{0} &\approx \mathbf{n} = \mathbf{N_{n,v}} \mathbf{N_{n,c}} (\Delta \mathbf{t} - \mathbf{T} \Delta \mathbf{s}) \\ \mathbf{0} &\approx \mathbf{r_m} = \epsilon \mathbf{A} (\mathbf{s_o} + \Delta \mathbf{s}). \end{aligned} \tag{9}$$

Implementing these fitting goals is problematic because of the space that $\Delta \mathbf{t}$ reside in. Unlike the Super Dix problem of Clapp (2003a), our data space is not regular. Normally our $\Delta \mathbf{t}$ values lie along a series of reflectors or a semi-random set of points (Clapp, 2001a). In either case, constructing $\mathbf{N_{n,c}}$ is problematic. When selecting points along reflectors, we are limited to a covariance description only along the reflectors with no easy way to describe continuity between reflectors. If we choose the random point methodology, we are limited to simply minimizing differences of nearby points, an unsatisfying option.

One solution to this problem is to introduce a mapping operator that maps $\Delta \mathbf{t}$ from an irregular space to a regular space. This solution holds promise, but the interaction between $\mathbf{N_{n,v}}$ and $\mathbf{N_{n,c}}$ becomes confusing.

Another option is to move the data variability problem. As mentioned earlier, our data isn't actually travel time differences, but γ values calculated by doing SRM. Normally we choose the γ value corresponding to the maximum semblance at a given location or some smooth version of the maximum (Clapp, 2003b). The selecting of the γ value is really where our data uncertainty problem lies. The selection problem has some convenient and some not so convenient properties. On the positive side, we are working with a regular grid and we know that we want some consistency along reflectors. As a result, a steering filter becomes a very obvious choice for our covariance description. On the negative side, the selection problem shares all of the non-linear aspects of the semblance problem (Toldi, 1985).

To get around these issues I decides to borrow something from both the geostatistics world and the geophysics world. Instead of thinking of the problem in terms of selecting the best γ value, I am going to think of the problem in terms of selecting a value within a distribution. I am going to construct my distributions in a similar manner to Rothman (1985). Rothman (1985) was trying to solve the non-linear residual statics problem using simulated annealing. He built a distribution based on stack power values from static-shift traces based on the surface locations of the sources and receivers. In this case, my distribution is going to be constructed based on the semblance values at given γ values.

I do not want the rough solution that Rothman (1985) was looking for, instead I am looking

for a smooth solution. If I set up the inverse problem

$$\begin{aligned} \mathbf{n} &\approx \mathbf{c} \\ \mathbf{0} &\approx \epsilon \mathbf{A}\mathbf{c}, \end{aligned} \tag{10}$$

I will get a vector $\mathbf{c}$ that contains random numbers that have been colored according to the spectrum of $\mathbf{A}$. I now have a field that has the spectrum I want but the vector $\mathbf{c}$ will tend to have a normal distribution with zero mean. At this stage, I am going to borrow something from the geostatistical community. When dealing with problems where the variable does not have a normal distribution, they use what they refer to as a normal-score transform (Isaaks and Srivastava, 1989; Deutsch and A.G., 1992). They build an operator $\mathbf{G}$ that relates a value a in an arbitrary distribution to a value c in standard normal distribution, $a = \mathbf{G}c$, based on the cumulative distribution function (cdf) of both distributions. I am going to apply the same trick. I will solve for all values of the variable $\mathbf{c}$ simutaneously and then apply $\mathbf{G}$ to convert these values to γ values.

From theory to practice

I found that squaring the semblance values $\text{semb}(\gamma)$ produced a better result than the semblance values themselves. My resulting cdf $a_{\text{cdf}}(\gamma_i)$ function was then

$$a_{\text{cdf}}(\gamma_i) = \frac{\sum_{\gamma_0}^{\gamma^i} \text{semb}^2(\gamma)}{\sum_{\gamma_0}^{\gamma^n} \text{semb}^2(\gamma)}. \tag{11}$$

In addition, I need to account for the fact that I am not scanning over all possible γ values. I introduced a constant parameter g_{max} that scaled my $\mathbf{c}$ values so that that one standard deviation of $\mathbf{c}$ might correspond to 2-5 standard deviations $\mathbf{a}$.

Finally, we are going to a precondition the model (Fomel et al., 1997) with the inverse of $\mathbf{A}$ and solve the problems in terms of the variable $\mathbf{p} = \mathbf{A}\mathbf{m}$,

$$\begin{aligned} \mathbf{n} &\approx \mathbf{A}^{-\mathbf{1}}\mathbf{p} \\ \mathbf{0} &\approx \epsilon \mathbf{p}. \end{aligned} \tag{12}$$

Limitations

The method described above isn't quite what we would like to have. Ideally we would rather phrase the problem as

$$\begin{aligned} \mathbf{n} &\approx \mathbf{G}\mathbf{A}^{-\mathbf{1}}\mathbf{p} \\ \mathbf{0} &\approx \epsilon \mathbf{p}, \end{aligned} \tag{13}$$

where $\mathbf{G}$ transforms our residual from the arbitrary distribution indicated by our semblance scan to a standard normal distribution. In this way we would be smoothing our semblance values rather than residual space shaping as indicated by fitting goals (12). The problem is that $\mathbf{G}$ can not be described in terms of a linear operator. If $\mathbf{G}$ was a stationary function we also wouldn't have a problem.

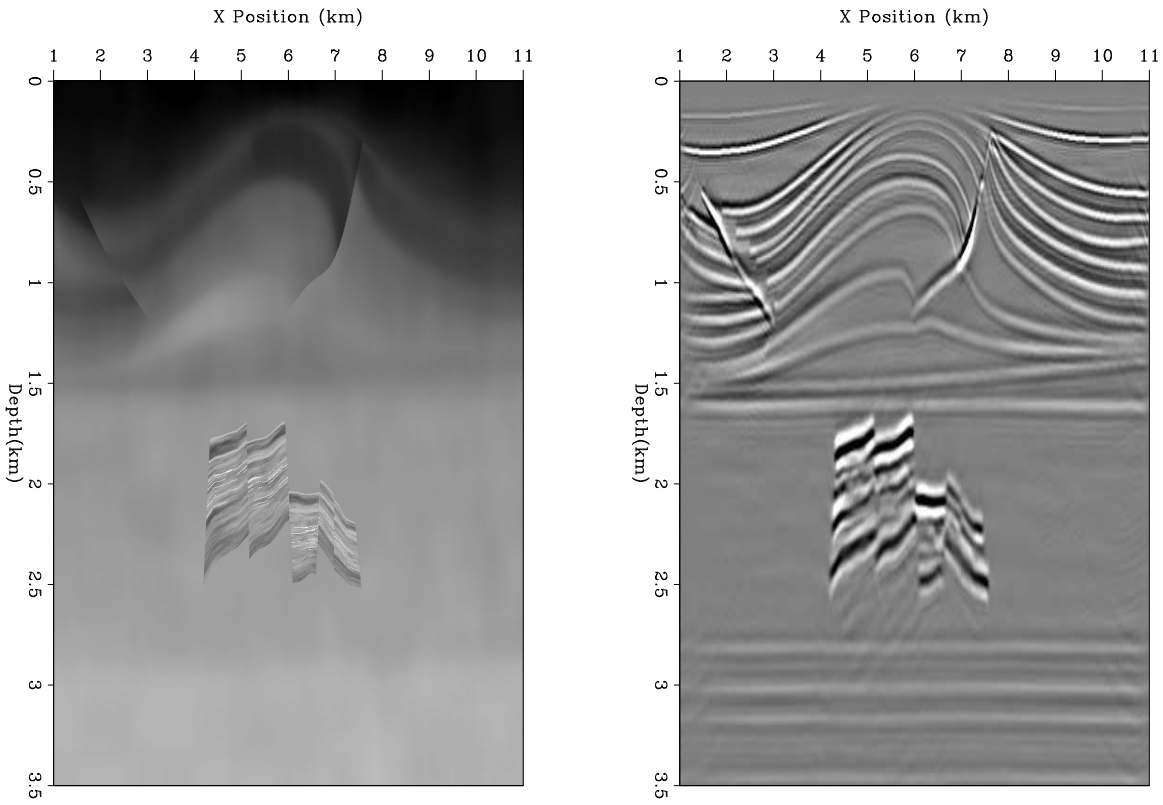

Figure 1: A 2-D synthetic. A realistic reservoir bounded by a faulted anticline and a basement rock. The left panel shows the velocity, the panel is the result of migrating with the correct velocity. bob3-correct [CR,M]

EXAMPLE

To test the methodology, I started with a fairly complex 2-D synthetic. The synthetic, shown in Figure 1, contains a realistic reservoir bounded by a faulted anticline and a basement rock. The velocity generally follows structure but with some low spatial frequency anomalies that range up to 5% of the background velocity. The synthetic reservoir is based on a real North Sea reservoir. The velocity and density structures vary significantly within the reservoir. The overburden was designed to break most conventional model characterization schemes. A layer-based approach would have difficulty with the anomalies and a gridded approach would find the sharp contrasts introduced by the faulting troublesome.

As an initial velocity estimate, I smoothed significantly the correct model. Figure 2 shows the initial velocity and the resulting migration. The basement reflectors are no longer flat and the anticline structure is more compressed in shape. The common reflection point gathers, five of which are shown in Figure 3, show significant move-out.

I then performed SRM semblance analysis on the dataset using γ ranging from .7 to 1.3. Figure 4 shows the semblance scans for the same five locations as in Figure 3. I used the initial migration image to construct a steering filter for the colored random number generation.

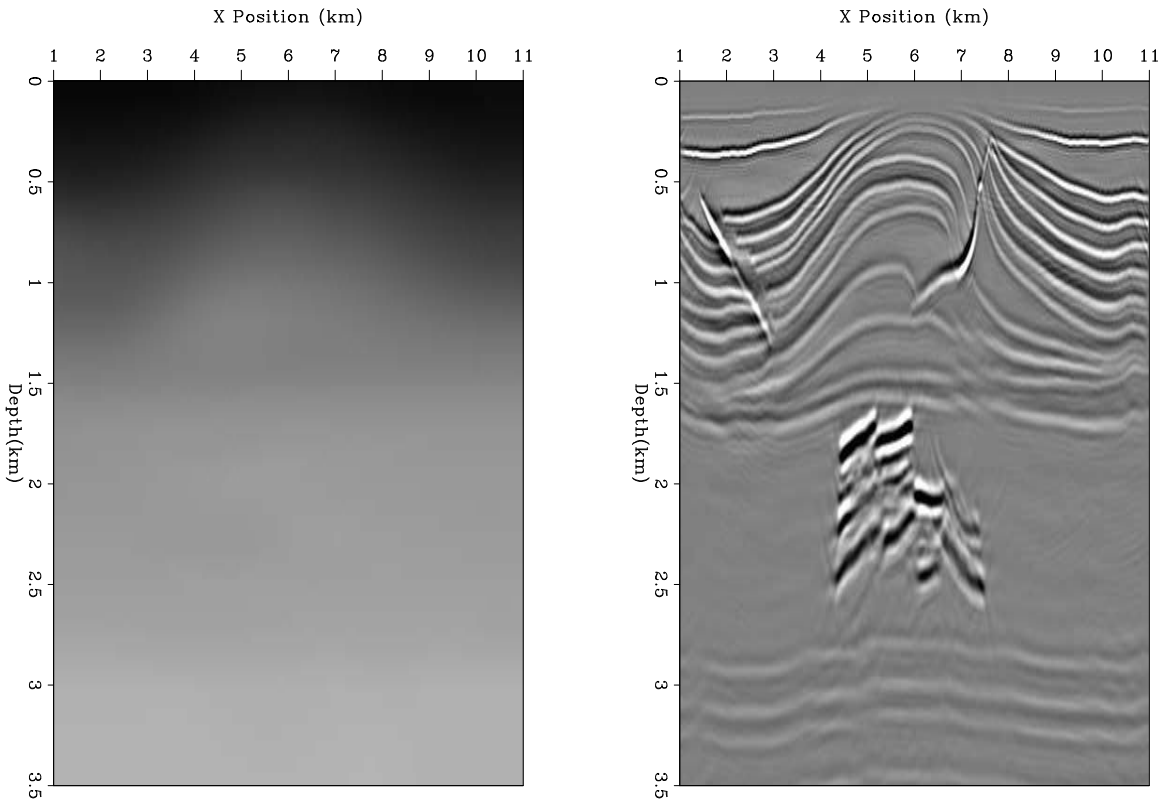

Figure 2: The left panel shows the initial velocity model. The right panel shows the resulting of migrating with this velocity model. bob3-initial [CR,M]

Figure 5 shows nine realizations of applying fitting goals (12). Note how the generated random numbers follow the image structure shown in Figure 2, but vary dramatically from realization to realization. I converted these random numbers to γ values using cdfs generated at every location using equation (11). Thirty realizations of γ values overlay the semblance scans in Figure 4. The various realizations are smooth as function of depth, which is reasonable. The amount of variance also seems reasonable. Note how when we have a sharp semblance maximum we see almost no variation, while when our blob is more spread out, the selected gamma values are more diverse. Note the fourth from the left gather at 1.8 seconds. Two different maxima are present in the semblance gather and we see that both are picked by various realizations. Figure 6 shows nine gamma maps as a function of space. The γ values are white when $\gamma = 1$ and become more red has γ becomes lower, and more blue as γ increases. Note how we see a spatial consistency within a panel but differences between the panels. The top-right portion of the various realizations is especially interesting. We see γ values greater than one, less than one, and some mix of both are selected by the various realizations.

The γ value were then used to update the velocity model using a preconditioned version of fitting goals (7). At this stage we are so far away from the correct answer that I limited the tomography to selecting back projection shallower than 1.7 km. Figure 7 shows the selected back projection points overlaid upon the migrated model. Figure 8 shows nine realizations of the tomography problem using the γ values shown in Figure 6. Note the variance in the

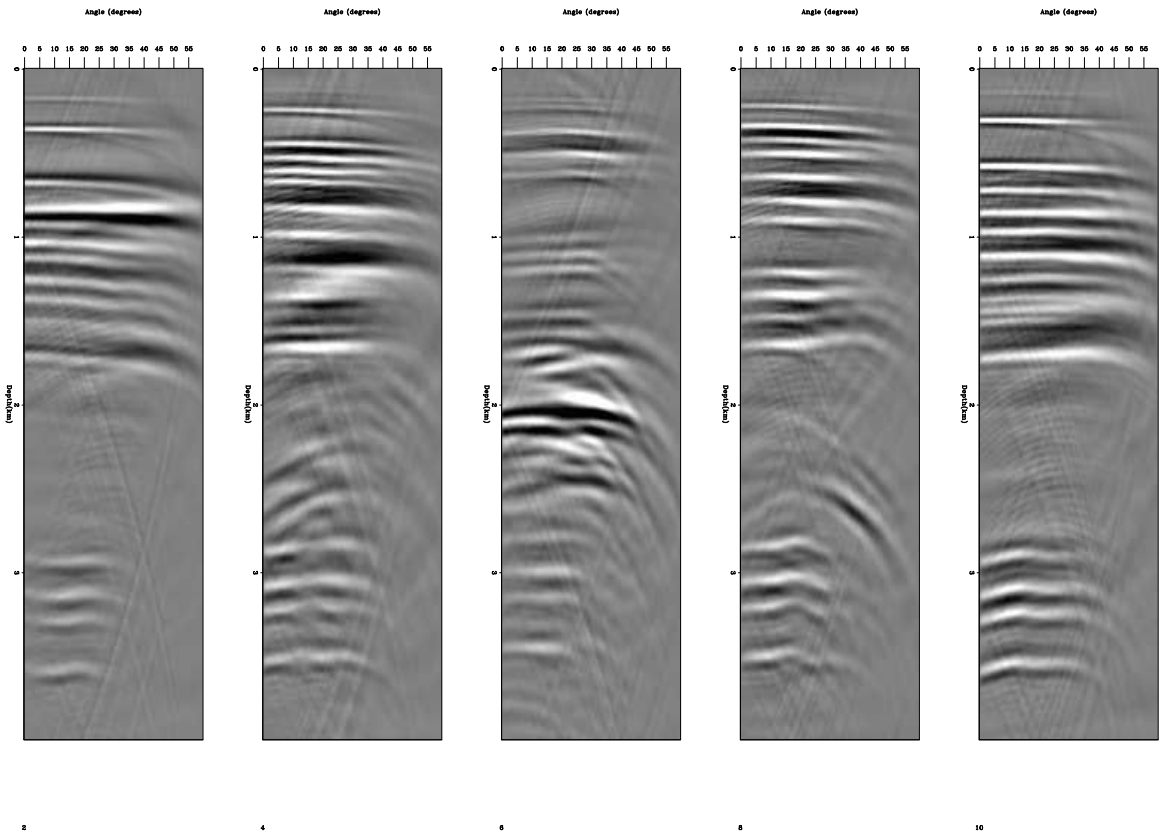

Figure 3: Five CRP gathers (X=2,4,6,8,10) using the velocity shown in the left panel of Figure 2. bob3-gathers [CR,M]

velocity structure from realization to realization. It is especially noticeable at the fault through the anticline and to the left the fault. We see velocity variations of $1km/s$ or greater between the various realizations. This isn't surprising given the variance present in our semblance scans (Figure 4).

As a final step, I migrated the data with the various velocity models. Figure 9 shows the nine images corresponding to the nine velocity models shown in Figure 8. Note the differences in the various images. The top-right image shows a much flatter basement reflector than any of the other realizations. The variation in positioning of the fault reflector is also significant between the various realizations.

CONCLUSION

The effect of velocity uncertainty on reflector positioning is assessed. Random numbers are colored using geologic dip information. These random numbers are used to select move-out descriptors which are in turn used in a reflection tomography problem. Initial results show that the methodology works as expected, but the variation when starting from such an

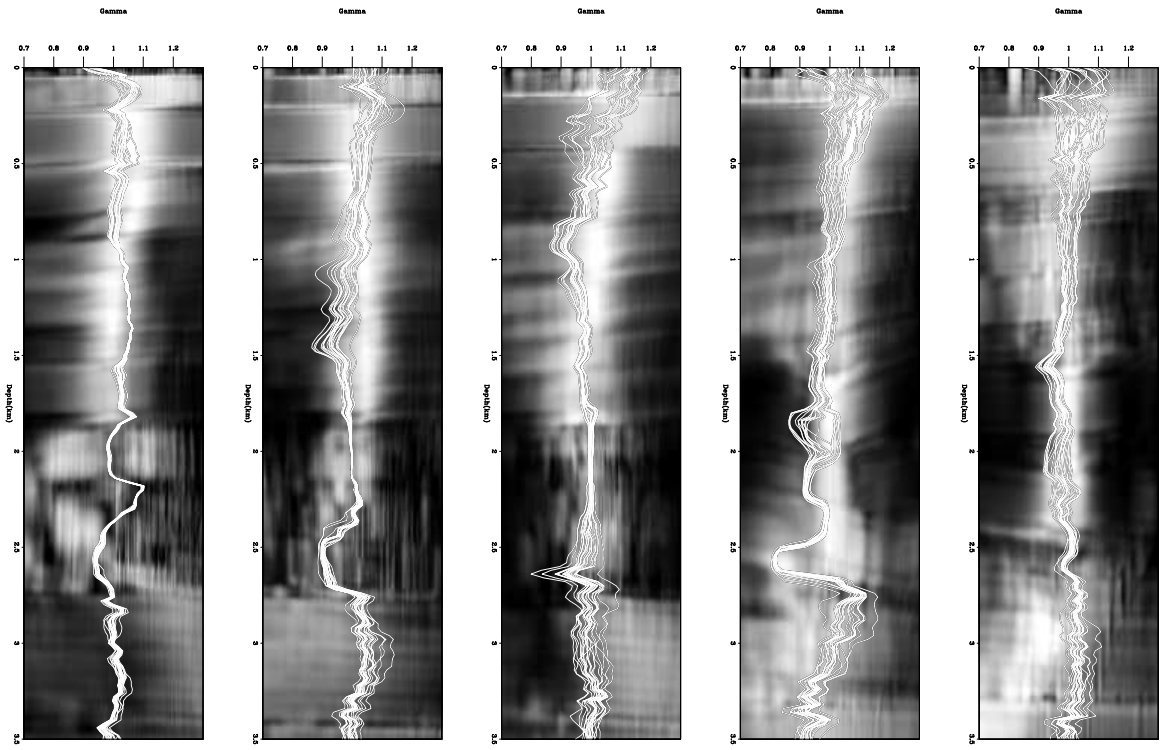

Figure 4: Five different SM semblance scans at the CRP locations shown in Figure 4. Overlaying the semblance scans are 30 different γ realizations. Note the fourth from the left gather at 1.8 seconds. Two different maxims are present in the semblance gather and we see that both are picked by various realizations. bob3-picks [CR,M]

erroneous initial velocity model causes large differences in the various image realizations. More meaningful results can be obtained when the estimated velocity is closer to the true velocity.

ACKNOWLEDGMENTS

I would like to thank Satomi Suzuki and Jef Caers of the Stanford Center for Reservoir Forecasting (SCRF) for providing the reservoir description used in this paper.

REFERENCES

Biondi, B., and Symes, W. W., 2003, Angle-domain common-image gathers for migration velocity analysis by wavefield-continuation imaging: Geophysics: submitted for publication.

Biondi, B., and Tisserant, T., 2004, 3-d angle-domain common-image gathers for migration velocity analysis: SEP–**115**, 163–190.

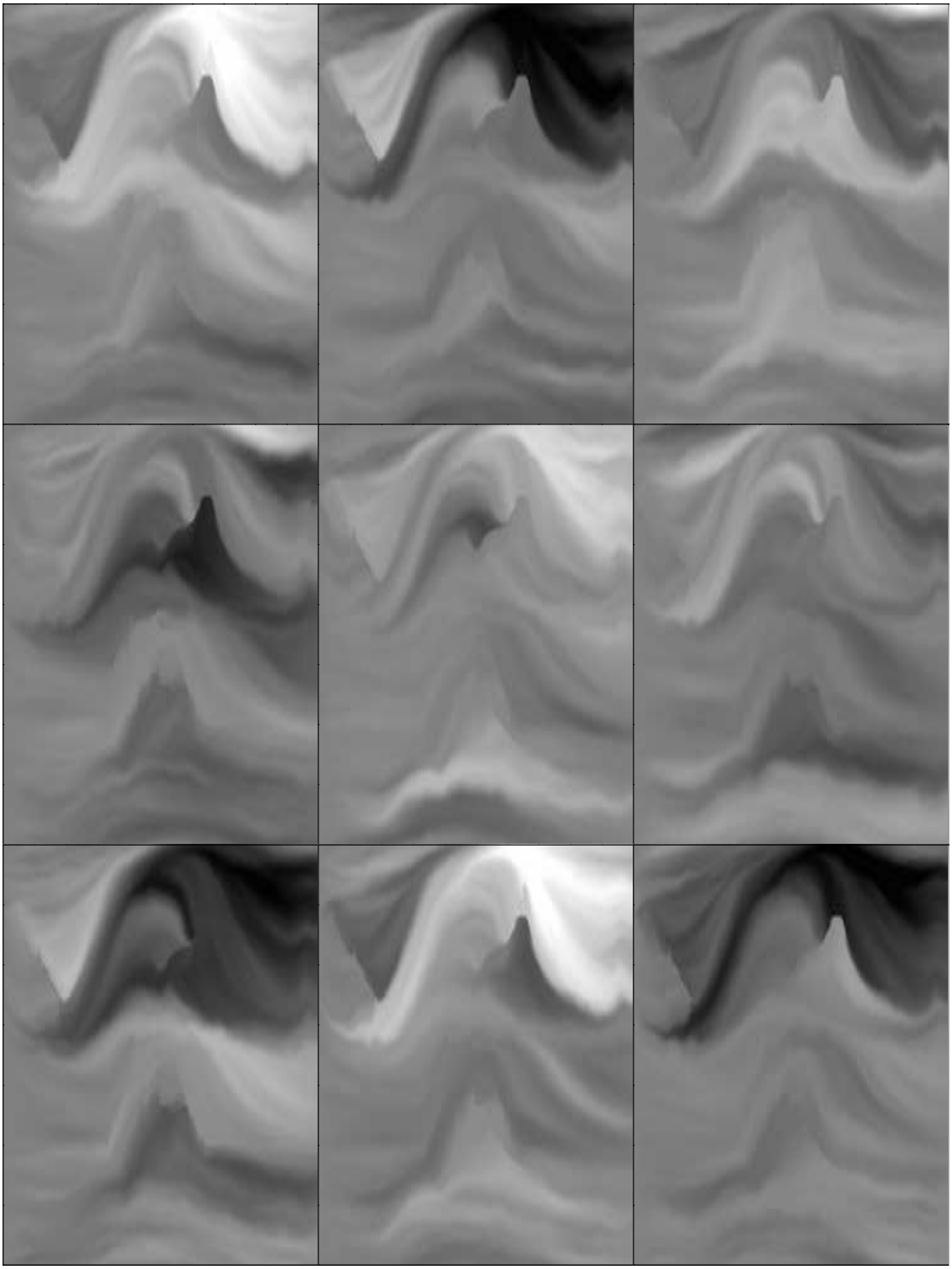

Figure 5: Nine realizations of random numbers colored by applying fitting goals (12). Note how the random numbers follow geologic dip but vary significantly from image to image. bob3-rand [CR,M]

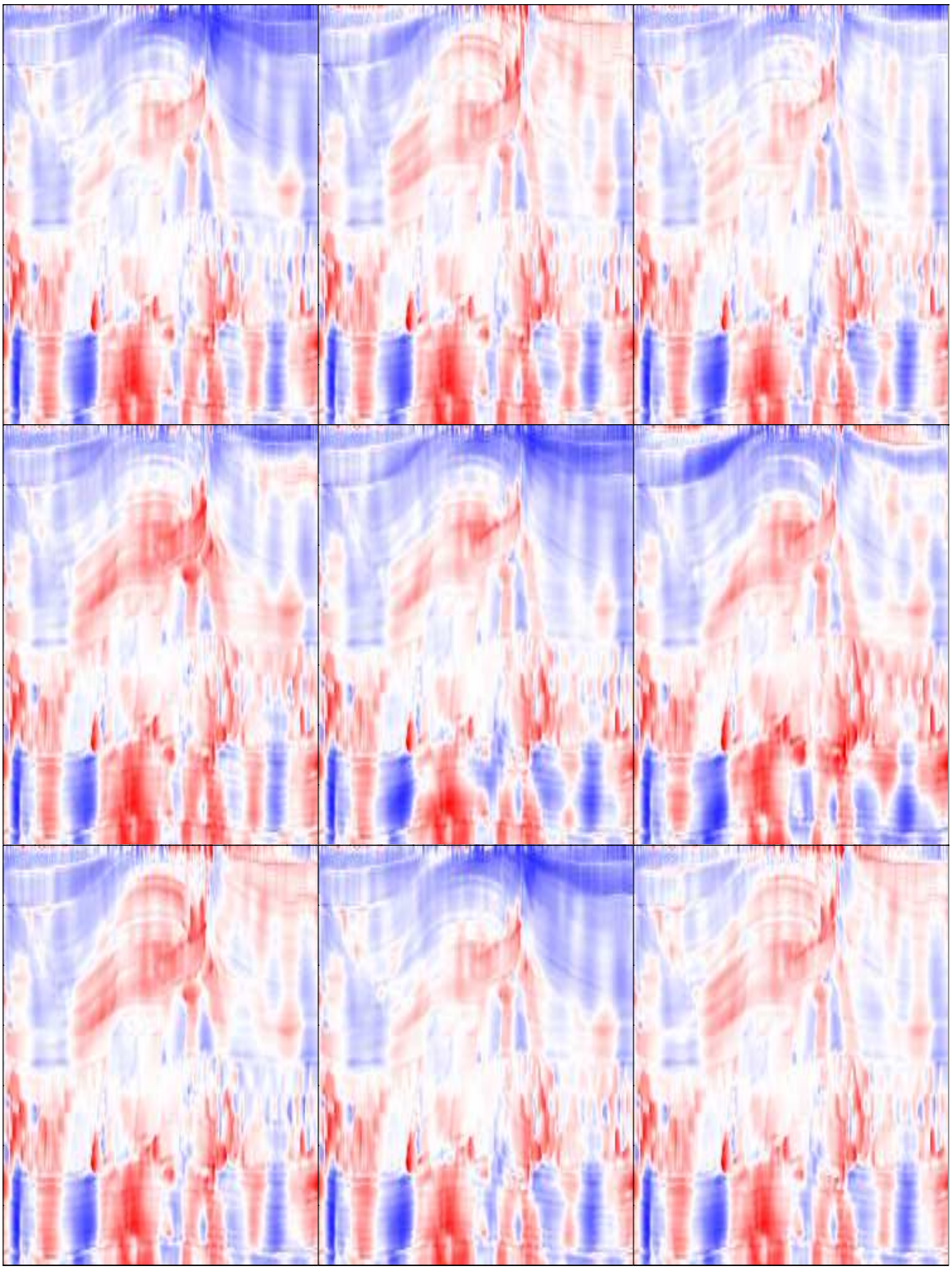

Figure 6: Nine realizations of γ values using the random numbers shown in Figure 5. Note how we see a spatial consistency within a panel but differences between the panels. bob3-gamma_mult [CR,M]

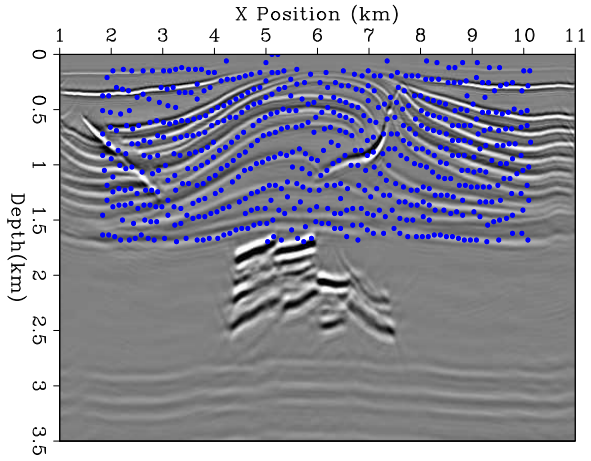

Figure 7: The points used to update the velocity model using ray-based tomography overlaying the initial migrated image. bob3-points [CR]

Chen, W., and Clapp, R., 2002, Exploring the relationship between uncertainty of ava attributes and rock information: SEP–**112**, 259–268.

Claerbout, J., 1999, Geophysical estimation by example: Environmental soundings image enhancement: Stanford Exploration Project, `http://sepwww.stanford.edu/sep/prof/`.

Clapp, R. G., and Biondi, B., 1999, Preconditioning tau tomography with geologic constraints: SEP–**100**, 35–50.

Clapp, R. G., Sava, P., and Claerbout, J. F., 1998, Interval velocity estimation with a null-space: SEP–**97**, 147–156.

Clapp, R., 2000, Multiple realizations using standard inversion techniques: SEP–**105**, 67–78.

Clapp, R., 2001a, Ray-based tomography with limited picking: SEP–**110**, 103–112.

Clapp, R. G., 2001b, Geologically constrained migration velocity analysis: Ph.D. thesis, Stanford University.

Clapp, R. G., 2001c, Multiple realizations: Model variance and data uncertainty: SEP–**108**, 147–158.

Clapp, R. G., 2002a, Effect of velocity uncertainty on amplitude information: SEP–**111**, 255–269.

Clapp, R. G., 2002b, Ray based tomography using residual Stolt migration: SEP–**112**, 1–14.

Clapp, R. G., 2003a, Multiple realizations and data variance: Successes and failures: SEP–**113**, 231–246.

Clapp, R. G., 2003b, Semblance picking: SEP–**113**, 323–330.

Cox, B., Winthaegen, P., and Verschuur, D., 2003, Combined cfp-based global and local velocity analysis applied to north sea data:, *in* 73rd Ann. Internat. Mtg. Soc. of Expl. Geophys., 2164–2167.

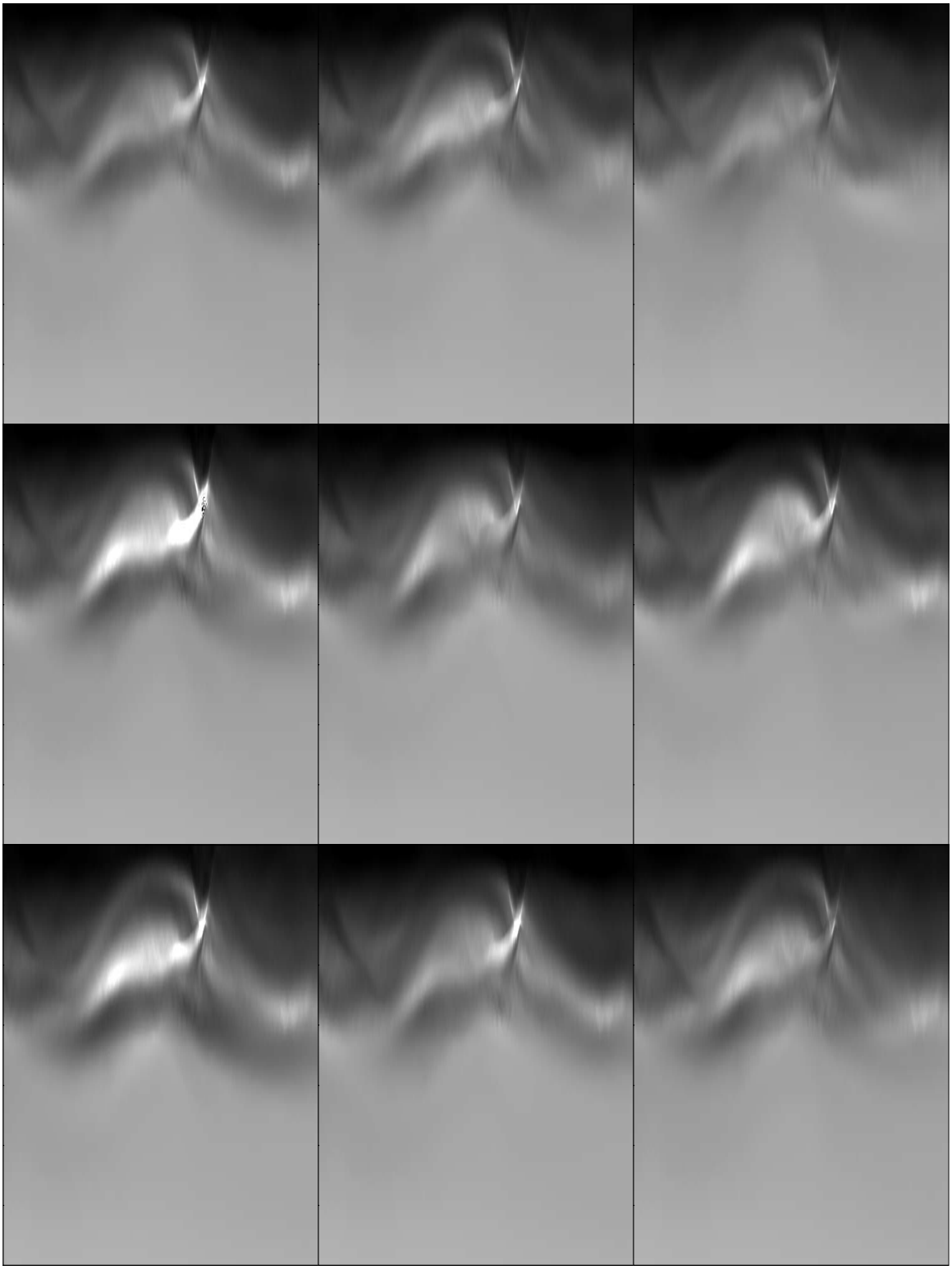

Figure 8: Nine realizations of tomography using the γ values shown in Figure 6. Note the variation in the velocity structure especially to the left of the fault cutting through the anticline. bob3-vel_mult [CR,M]

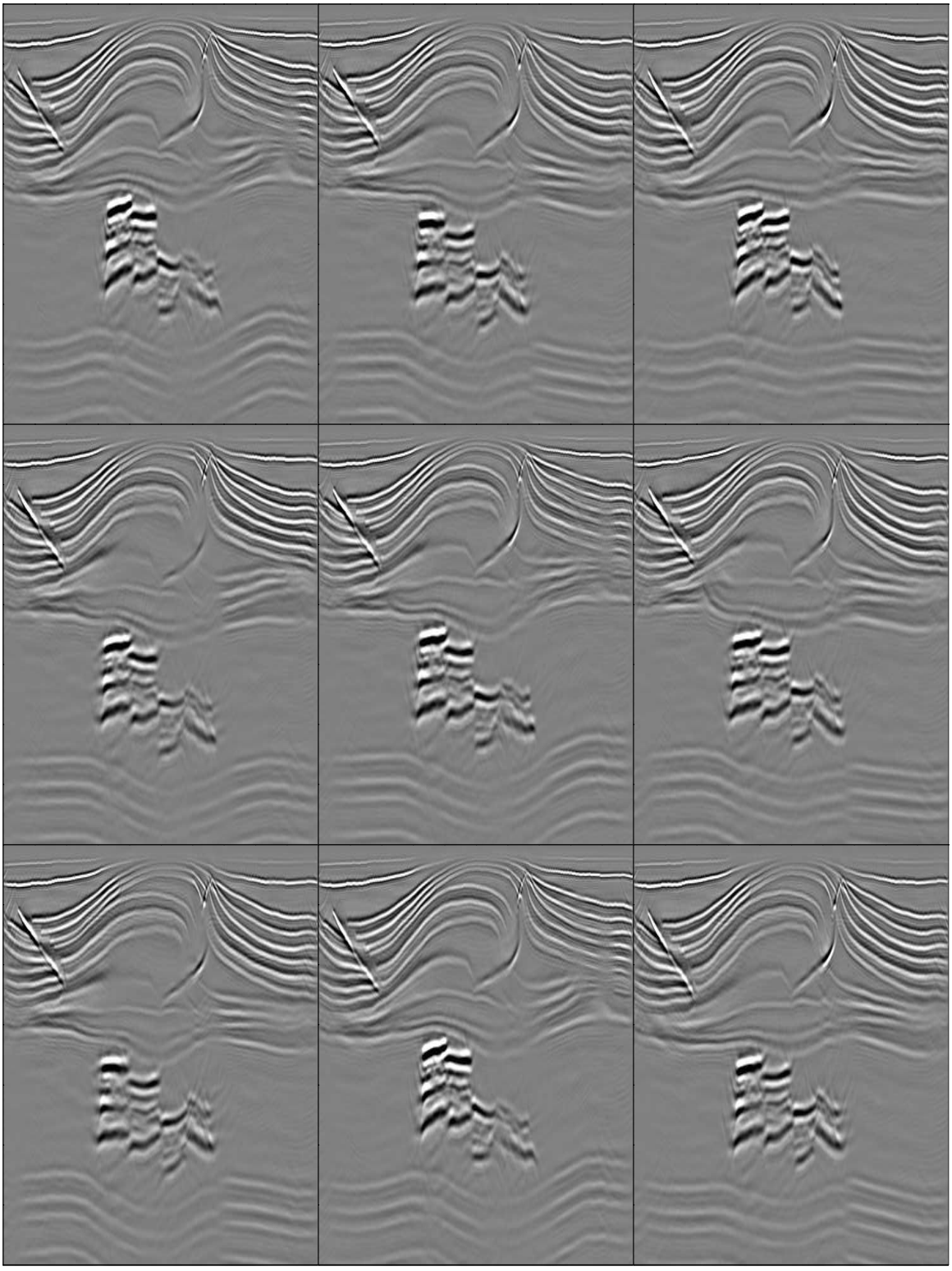

Figure 9: Nine realizations corresponding to the nine velocity models shown in Figure 8. Note the differences in the various images. The top-right image shows a much flatter basement reflector than any of the other realizations. The variation positioning of the fault reflector is also significant between the various realizations. bob3-image_mult [CR,M]

Crawley, S., 2000, Seismic trace interpolation with nonstationary prediction-error filters: Ph.D. thesis, Stanford University.

Deutsch, C. V., and A.G., J., 1992, GSLIB: Geostatistical software library and user's guide: Oxford University Press.

Fomel, S., Clapp, R., and Claerbout, J., 1997, Missing data interpolation by recursive filter preconditioning: SEP–**95**, 15–25.

Isaaks, E. H., and Srivastava, R. M., 1989, An Introduction to Applied Geostatistics: Oxford University Press.

Prucha, M. L., Biondi, B. L., and Symes, W. W., 1999, Angle-domain common image gathers by wave-equation migration: SEP–**100**, 101–112.

Ristow, D., and Ruhl, T., 1994, Fourier finite-difference migration: Geophysics, **59**, no. 12, 1882–1893.

Rothman, D. H., 1985, Large near-surface anomalies and simulated annealing: Ph.D. thesis, Stanford University.

Sava, P., and Fomel, S., 2000, Angle-gathers by Fourier Transform: SEP–**103**, 119–130.

Sava, P., 1999a, Short note–on Stolt common-azimuth residual migration: SEP–**102**, 61–66.

Sava, P., 1999b, Short note–on Stolt prestack residual migration: SEP–**100**, 151–158.

Stoffa, P. L., Fokkema, J. T., de Luna Freire, R. M., and Kessinger, W. P., 1990, Split-step Fourier migration: Geophysics, **55**, no. 4, 410–421.

Stork, C., and Clayton, R. W., 1991, An implementation of tomographic velocity analysis: Geophysics, **56**, no. 04, 483–495.

Tarantola, A., 1987, Inverse Problem Theory: Elsevier Science Publisher.

Toldi, J., 1985, Velocity analysis without picking: Ph.D. thesis, Stanford University.